Aalborg Universitet

AALBORG UNIVERSITY
DENMARK

Water-Structure Interactions on a Point Absorber

Jakobsen, Morten Møller

Publication date:
2015

Document Version
Accepted author manuscript, peer reviewed version

Link to publication from Aalborg University

Citation for published version (APA):
Jakobsen, M. M. (2015). *Water-Structure Interactions on a Point Absorber*. Department of Civil Engineering, Aalborg University. DCE Technical reports No. 183

General rights
Copyright and moral rights for the publications made accessible in the public portal are retained by the authors and/or other copyright owners and it is a condition of accessing publications that users recognise and abide by the legal requirements associated with these rights.

- Users may download and print one copy of any publication from the public portal for the purpose of private study or research.
- You may not further distribute the material or use it for any profit-making activity or commercial gain
- You may freely distribute the URL identifying the publication in the public portal -

Take down policy
If you believe that this document breaches copyright please contact us at vbn@aub.aau.dk providing details, and we will remove access to the work immediately and investigate your claim.

Downloaded from vbn.aau.dk on: April 19, 2024

Water-Structure Interactions on a Point Absorber

Morten Møller Jakobsen

DEPARTMENT OF CIVIL ENGINEERING
AALBORG UNIVERSITY

ISSN 1901-726X
DCE Technical Report No. 183

Aalborg University
Department of Civil Engineering
Wave Energy Research Group

DCE Technical Report No. 183

Water-Structure Interactions on a Point Absorber

by

Morten Møller Jakobsen

February 2015

© Aalborg University

Scientific Publications at the Department of Civil Engineering

Technical Reports are published for timely dissemination of research results and scientific work carried out at the Department of Civil Engineering (DCE) at Aalborg University. This medium allows publication of more detailed explanations and results than typically allowed in scientific journals.

Technical Memoranda are produced to enable the preliminary dissemination of scientific work by the personnel of the DCE where such release is deemed to be appropriate. Documents of this kind may be incomplete or temporary versions of papers—or part of continuing work. This should be kept in mind when references are given to publications of this kind.

Contract Reports are produced to report scientific work carried out under contract. Publications of this kind contain confidential matter and are reserved for the sponsors and the DCE. Therefore, Contract Reports are generally not available for public circulation.

Lecture Notes contain material produced by the lecturers at the DCE for educational purposes. This may be scientific notes, lecture books, example problems or manuals for laboratory work, or computer programs developed at the DCE.

Theses are monograms or collections of papers published to report the scientific work carried out at the DCE to obtain a degree as either PhD or Doctor of Technology. The thesis is publicly available after the defence of the degree.

Latest News is published to enable rapid communication of information about scientific work carried out at the DCE. This includes the status of research projects, developments in the laboratories, information about collaborative work and recent research results.

Published 2015 by
Aalborg University
Department of Civil Engineering
Sofiendalsvej 11,
DK-9200 Aalborg SV, Denmark

Printed in Aalborg at Aalborg University

ISSN 1901-726X
DCE Technical Report No. 183

Recent publications in the DCE Technical Report Series

ISSN 1901-726X
DCE Technical Report No. 183

Contents

Preface **ix**

Introduction **1**

1 Current Flumne **3**
1.1 Method . . . 3
1.2 Results . . . 3
1.3 Discussion . . . 4

2 Wave Basin **7**
2.1 Introduction . . . 7
2.1.1 Setup . . . 8
2.1.2 Wave Conditions . . . 9
2.2 Methods . . . 10
2.3 Results . . . 11
2.4 Discussion . . . 16

Conclusion **17**

Bibliography **19**

A Instrumentation and Data Acquisition in Wave Basin **21**
A.1 The Float and embedded sensors . . . 21
A.2 Force and Torque transducer . . . 22
A.3 Simulink and XPC data acquisition . . . 22
A.4 Surface Elevation and Velocimetry . . . 23
A.5 The Basin and Wave Series . . . 25

Preface

All experiments in this report is from sessions in the current flume and wave basin at Aalborg University. The experiments span two years, 2012-2013, with experiments repeated in both the flume and basin. Only the most recent experiments are presented.
The experiments were carried out with Morten Mejlhede Kramer and technicians Nikolaj Holk and Niels Drustrup throughout the experiments. Other researchers involved in the experiments includes, Francesco Ferri, Scott Beatty, Morten Thøtt Andersen, Thomas Viuff and Oana Coman.

Morten Møller Jakobsen
mmj@civil.aau.dk
http://homes.civil.aau.dk/mmj/
Sofiendalsvej 11, Room: 11.218
9000 Aalborg

Introduction

This technical report presents experiments carried out in the current flume and wave basin at Aalborg University in 2012 and 2013. The results of the experiments were not satisfactory, and hence was never published as neither conference nor journal. However, the experience from the experiments has been the primary catalyst to more successful work later and may be helpful to others working in laboratory.

The purpose of the experiments is to examine the wave and current induced loads on a floating point absorber (wave energy converter). Wave energy converters are used in ocean- or costal regions where significant wave loads occur. This means that wave loads will be the governing force to account for, which will typically mean that forces are inertia dominated with some drag contribution. The results presented will determine the magnitude of these load components using Morison's equation.

First chapter determines the drag component using a variety of current velocities in the stream canal. Second chapter primarily determines the inertia component from regular wave experiments in the wave basin. The contribution from drag is estimated in the later and compared with those found in the former.

Chapter 1

Current Flumne

The primary purpose of the experiments in the current flume was to determine the drag coefficient of the hemisphere. This was strongly motivated by the anticipation difficulty in separating drag from the inertia-dominated waves in the basin.

1.1 Method

The setup in the current flume is seen in Fig. 1.1a, with the dimensions of the float in Fig. 1.1c. It consisted of a 25 cm Styrofoam hemisphere with a painted surface with a 6-axis load-cell on top. During the experiments, the float was kept in place using an overlaying crossbeam. The level of submersion was closely monitored to ensure that the wetted surface area remained constant. The velocity was measured 5 cm below the water surface using both a propeller and from ultrasonic measurements cf. Fig. 1.1b.
In pure current the drag coefficient is calculated using Eq. 1.1 and the Reynolds Number from Eq. 1.2.

$$C_D = \frac{F_y}{0.5 \cdot \rho \cdot u^2 A} \tag{1.1}$$

$$Re = \frac{u \cdot D}{\mu} \tag{1.2}$$

1.2 Results

Undisturbed velocity profiles were made with low- and mid-range velocities cf. Fig. 1.2.

Using Eq. 1.1 the drag-coefficients were plotted with Reynolds numbers in Fig. 1.3. Additional results were included from experiments carried out with a similar setup in 2008.

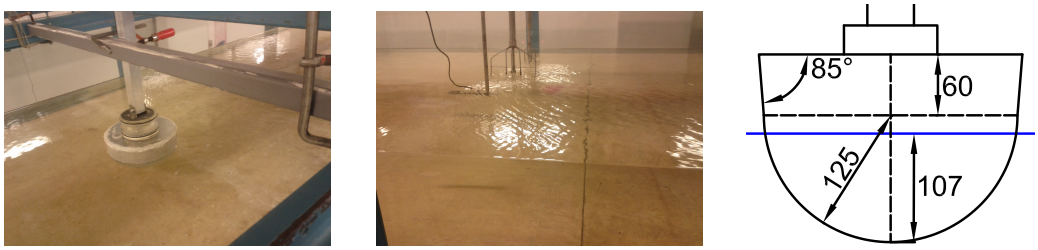

(a) Float and mount. **(b)** Velocimeters. **(c)** Float proportions.

Figure 1.1: Experimental setup in flume in Aalborg. Measurements in mm.

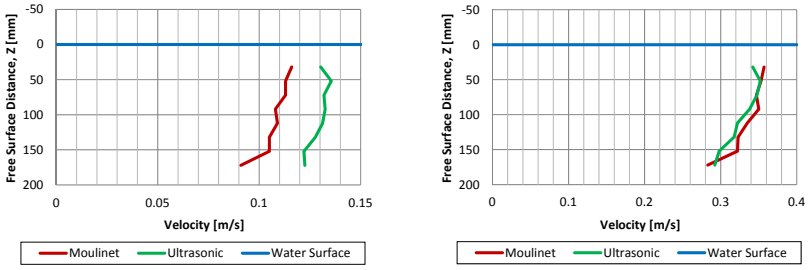

(a) $u \approx 0.125$ m/s. **(b)** $u \approx 0.345$ m/s.

Figure 1.2: Velocity profile in low- and mid-range currents.

1.3 Discussion

The water level in the flume was kept rather high compared to normal operation, to limit the effect of the boundary layer. This had the adverse effect that the pump would reach maximum capacity. This led to some unfortunate time dependent fluctuations in the velocity, and from observations, a rapidly increasing turbulence. These data was discarded and set the upper limit on the velocity range.
As seen in Fig. 1.2a, the lower velocities caused the propeller to deviate quite severely from the ultrasonic measurements. This was attributed to friction in the propeller. For velocities lower than 0.2m/s the propeller measurements was discarded. With velocities greater than 0.2 m/s the deviation between the two was less than 5%. With these limitations the velocity range still covered 0.08 to 0.72 m/s equivalent to a Reynolds range of $2.36 \cdot 10^4$ to $1.82 \cdot 10^5$ seen in Fig. 1.3.

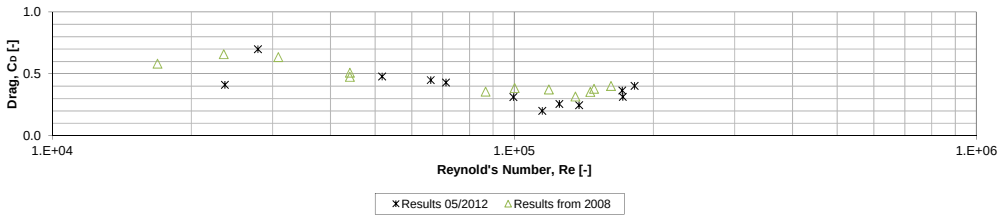

Figure 1.3: Drag coefficient from stream canal experiments.

Chapter 2

Wave Basin

Experiments are performed in both current flume and wave basin to determine current and wave interactions with a hemispherical point absorber. Firstly an investigation is performed on the device to determine the influence of drag and inertia forces in various wave conditions for the specific device. Secondly it is shown how the causal control of the floats motions will affect the fluid-structure interactions.

2.1 Introduction

Established developers of renewable energy devices have long been struggling to be economically feasible alternatives to fossil fuels. This is a steep challenge for emerging industries such as wave energy, which is still attempting to bring their models to a commercial stage. The measurement typically used is the cost of energy, which includes, structural costs, operation and maintanance. To reduce structural cost, cheaper production materials and production methods are often considered.
The glass-fiber and steel structure solutions that has been used so far is an expensive solution. For the Wavestar device an alternative is considered using reinforced concrete for the arm and fiber-reinforced concrete for the shell. A significant drawback of concrete when used in this context is the weight. The own weight affects the system when the floats needs to be pulled out of the water during storm protection (where the device jacks further up for protection against the waves). For the half scale prototype, the solution is to increase the size of the cylinder lifting. The larger cylinder size increases the initial cost, operation and reduce the efficiency. This is however offset by the decrease in the float and arm expenses. Reducing the expenses further can be done by increasing the knowledge of the loads on the float. This report seeks to study these forces both with the float in a stationary (locked) position but some initial evaluation of the effects of causal control strategies (i.e. Hansen and Kramer (2011)) are considered too.
This paper will present the results of experiments with a small scale device (1:40 of full scale). Both drag and inertia contributions are examined in heave and surge (wave propagation direction) in regular wave series. These coefficients are deter-

mined by locking the device in its natural buoyancy position to limit uncertainties. To determine the wave excitations on an active WEC the device is released from the locked position to allow it to oscillate freely within the confines of the arm and ball bearings. The way this is done is by not applying any force to the actuator. In this so-called free float state the regular wave series are repeated.
The third state tested is done using a causal controlled Power Take-Off (PTO) system. The PTO is not optimized for the waves in these experiments.

2.1.1 Setup

The device used is a new hemispherical float made in glass fibre shown in Fig. 2.1. The float has a diameter of 250mm which is a scale 1:20 of the Wavestar device installed at Hanstholm harbor in Denmark, eg. Kramer et al. (2011). The scale of the device has been chosen to correspond to the constraints given by the wave basin. The basin dimensions are 15.7m x 8.5m x 1m which allows for 0.65m water depth and wave heights of about 0.30m. For additional information on the instrumentation see Appendix A.

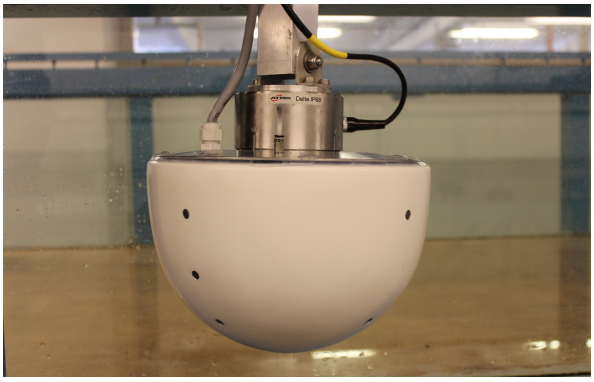

Figure 2.1: Hemisphere with 6-axis F/T-transducer and pressure sensors installed.

In the wave basin the device is connected to a frame on the platform above the basin, see Fig. 2.2. It consists of an arm extending at a fixed angle from the device to a bearing at the vertical support. The PTO control is implemented using a linear magnetic actuator.

To measure the environmental conditions that the device is subjected to both resistive wave gauges and an Acoustic Doppler Velocimeter (ADV) are used. The measuring equipment used to monitor the excitation and the response of the device is a six Degree of Freedom (DoF) F/T sensor positioned between arm and float. An additionally pressure transducers mounted in the surface of the device. The measurements of the pressure gauges will be omitted in this paper. The PTO force is determined using a force sensor placed between arm and the cylinder of the actuator. A laser displacement sensor is used to measure the position of the cylinder, which is

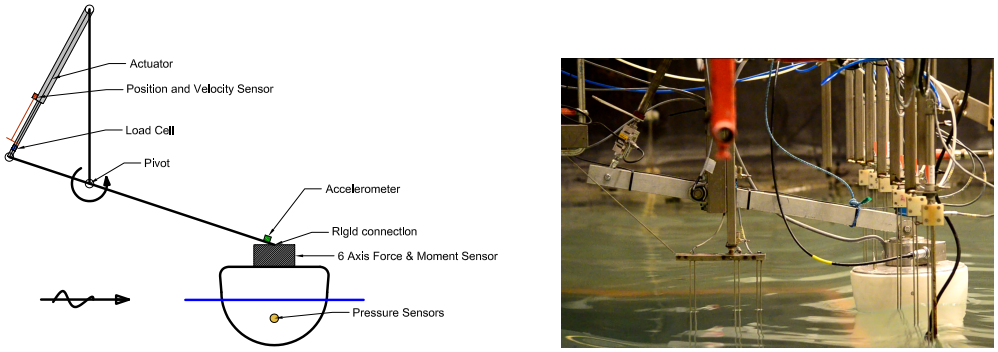

(a) Experimental concept. **(b)** Experimental setup.

Figure 2.2: Setup used during experiments in the wave basin.

used to determine angular velocity and acceleration of the arm by kinematic relations. This is cross-checked using an accelerometer located in the same location as the F/T sensor. Due to the extra measuring equipment the float is too heavy to float correctly in the water by buoyancy alone. To compensate for the extra weight it has been necessary to apply a proportional uplifting moment in the ball bearings, which is achieved by applying a dynamic force offset to the actuator's control system.

2.1.2 Wave Conditions

For regular/monochromatic waves a total of 46 unique waves of varying wave heights and periods are used. The wave series reaches the upper and lower bounds of what is possible to make in the basin. At the selected water depth the bounds supplied to the wave generation software are wave heights between $H = 0.02 - 0.31$ m and periods from $T = 0.7 - 2.0$ s which leads to wave with steepness factors in the range of $s = 0.01 - 0.10$. This leads to a distribution of regular waves as shown in Fig. 2.3.

The wave makers are set to run each regular wave series for 60 seconds and rest for 45 seconds between each test. This is decided to be sufficient to determine the interactions with regular waves as reflections from the beach will affect the results. Each test is run for each of the three cases with the float in place and once with no float to use as an undisturbed reference. For irregular/panchromatic waves it is sought to provide a comparable scenario for all the wave series. This is done by using a common reference wave series; which is made with unit properties $H_{m0} = 1$ m and $T_p = 1$ s. By using a white noise filtering method it is ensured that the wave series are non-deterministic. The frequency spectrum is a parameterised Pierson-Moskowitz spectrum. The sample length is chosen to be $l_s = 1200 \cdot T_p$ with a sampling frequency $f_s = 109.23$ Hz which is convenient when generating the signal in the wave making software which uses the inverse FFT and the original phases to approximate the requested signal. By choosing this sampling frequency the block size is a power of two $N = l_s \cdot f_s = 2^{17}$.

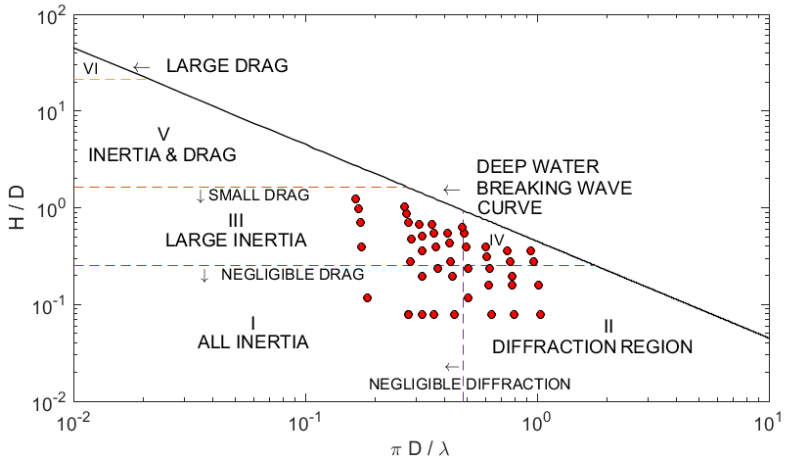

Figure 2.3: Wave regime Chakrabarti (1987).

The values of the reference wave series is then scaled in magnitudes based on the wave heights needed and the peak wave period is adjusted by changing the sampling frequency used by the wave generation software.

2.2 Methods

The regular wave series are reduced to 10 succeeding waves to reduce the influence of reflection from the beach. The waves are chosen as the first wave surpassing 3/4th of the largest wave in each wave series. This has shown to be enough waves to accurately determine the wave properties.
Some wave series was improperly produced in the basin, resulting in misshaped profiles in the far field in the testing area. This happened with wave periods $T > 1.4$ s and for series with very high or low wave heights. As high order wave theory is used to determine the velocities these series has been removed in the results presented.
To obtain continuous measurements of fluid particle velocity from the waves, the ADV was placed 20 cm below the water surface so it would not protrude through the surface during wave troughs. However; the fluid particle velocity of interest for the Float is 10 cm below the water surface at the centroid of the submerged volume. Thus, the stream function wave kinematic theory by Dean (1965) (With modifications by Chaplin (1980) and Brorsen (2007)) was validated using of the ADV measurements at 20 cm water depth, then used to calculate the velocity at the WEC (10 cm depth).
For some of the steeper waves it was not possible to reach convergence, regardless of the number of Stream functions used. When no convergence was possible Stoke's 5th order theory by Fenton (1985) was used instead.
Both of the high order wave models are dependent of determining the characteristic

wave heights and periods. These characteristics was determined using a time domain model on the wave series. The velocities was first calculated for 20 cm water depth to ensure that the theoretical approximations used to calculate the velocity corresponeded with the ADV. The standard deviations for all samples are $\sigma^2 < 0.01$.

It is sought to determine the contributions from drag, C_D, and inertia, C_M, in both vertical and horizontal wave propagation direction. This is done by locking the float, measuring the excitation forces using Morison's equation in Eq. 2.1 and then estimating the coefficients.

$$F_p = \frac{1}{2} C_D \rho A u|u| + C_M \rho V \frac{Du}{Dt} \tag{2.1}$$

Two methods are used to obtain the coefficients. The first method determines the coefficients by methodically running through ranges of realistic drag and inertia coefficients in the Morison's equation (Brute force). The best solution is determined by calculating the minimum variance (MV) between measured force F_m and "predicted" F_p. This effectively leads to one solution for each regular wave. The second method proposed by Dean and Dalrymple (1984) seeks to obtain the two coefficients by an least squares optimum fit approach (LS). This is done using the minimum squared error between the predicted force F_p and the measured force F_m shown in Eq. 2.2. The analytical gradients of the objective function with respect to the unknowns C_D and C_M are shown in Eq. 2.3.

$$\epsilon^2 = \frac{1}{I} \sum_{i=1}^{I} \left(F_{m,i} - F_{p,i}\right)^2 \tag{2.2}$$

$$\begin{aligned} \frac{\partial \epsilon^2}{\partial C_D} &= \frac{2}{I} \sum_{i=1}^{I} \left(F_{m,i} - F_{p,i}\right) \frac{\partial F_{p,i}}{\partial C_D} = 0 \\ \frac{\partial \epsilon^2}{\partial C_M} &= \frac{2}{I} \sum_{i=1}^{I} \left(F_{m,i} - F_{p,i}\right) \frac{\partial F_{p,i}}{\partial C_M} = 0 \end{aligned} \tag{2.3}$$

To obtain the particle velocity used in Eq. 2.1 the previously mentioned wave theory is used to determine the velocity at the center of the float. In Eq. 2.4 the simple PI control scheme used is shown. The values are not optimized for the individual regular wave series, but kept constant ($k = -50$ and $c = 10$).

$$f_c(t) = c \cdot \dot{\theta}(t) + k \cdot \theta(t) \tag{2.4}$$

2.3 Results

The results of the two methods used to estimate the drag and inertia coefficients in surge are shown in Fig. 2.4. By minimizing the variance between the MV method produces coefficients for each wave series. With the LS fit each regular series is divided into bins based on Reynolds Number.

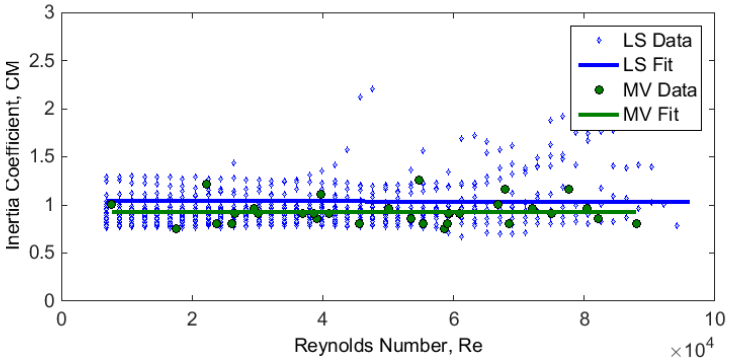

(a) Inertia.

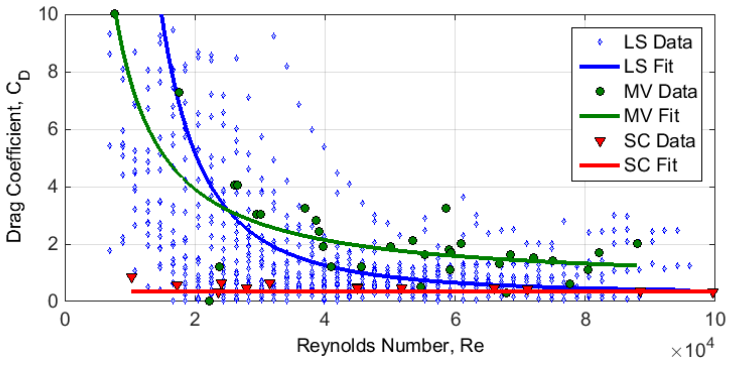

(b) Drag.

Figure 2.4: Drag and inertia coefficients obtained from the regular wave series in the wave propagation direction. Data point are shown with best fitting tendency lines.

The results obtained from calculation of the coefficients in heave are shown in Fig. 2.5.

The measured forces are plotted against the corresponding wave heights in Fig. 2.6 and periods in Fig. 2.7. The hydrostatic force has been removed from the results. In Fig. 2.8 the forces are normalized using Froude-Krylov.

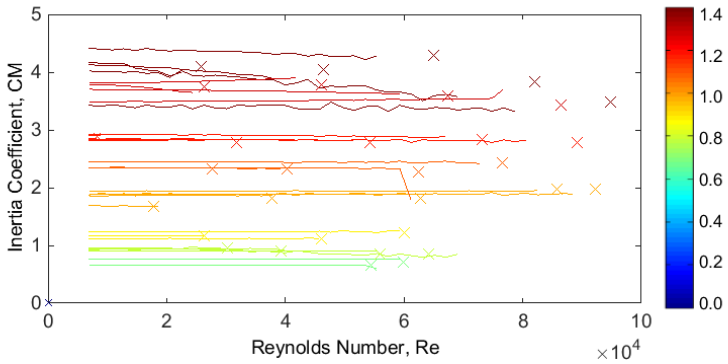

(a) Inertia. The wave periods of the waves are indicated by the color gradient. The solid lines represent one wave series analyzed using the LS fitting method and the crosses are the calculated values from the MV method.

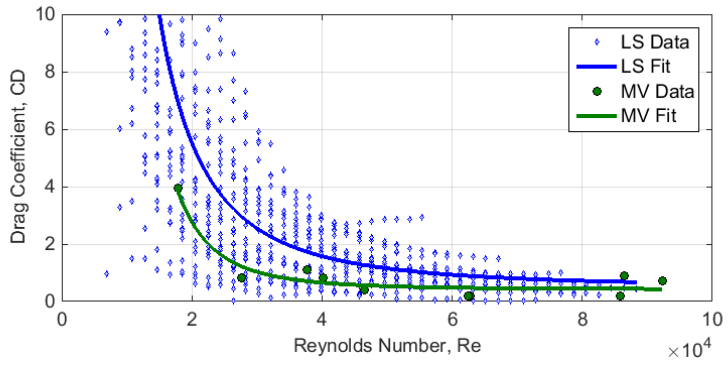

(b) Drag coefficients with data point are shown with best fitting tendency lines.

Figure 2.5: Drag and inertia coefficients obtained from the regular wave series in vertical direction.

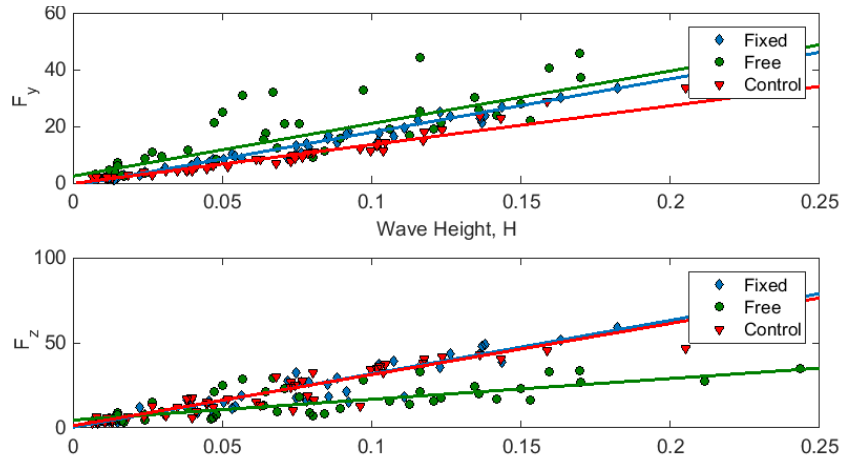

Figure 2.6: Measured forces on float for the regular wave series.

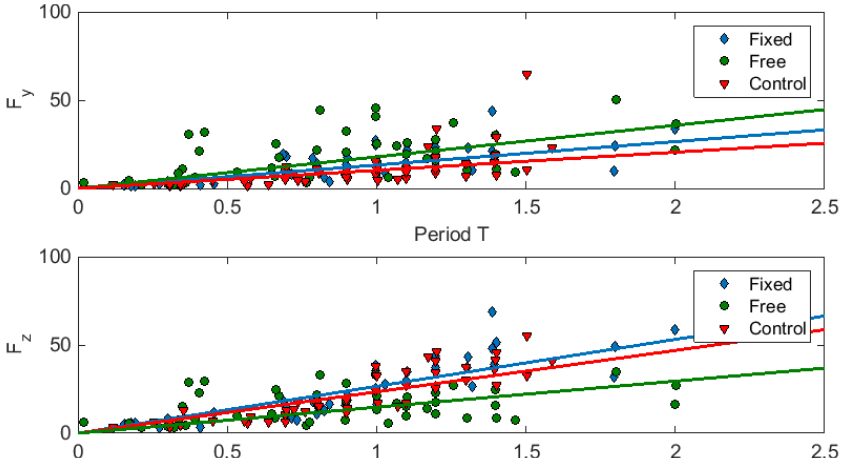

Figure 2.7: Measured forces on float for the regular wave series.

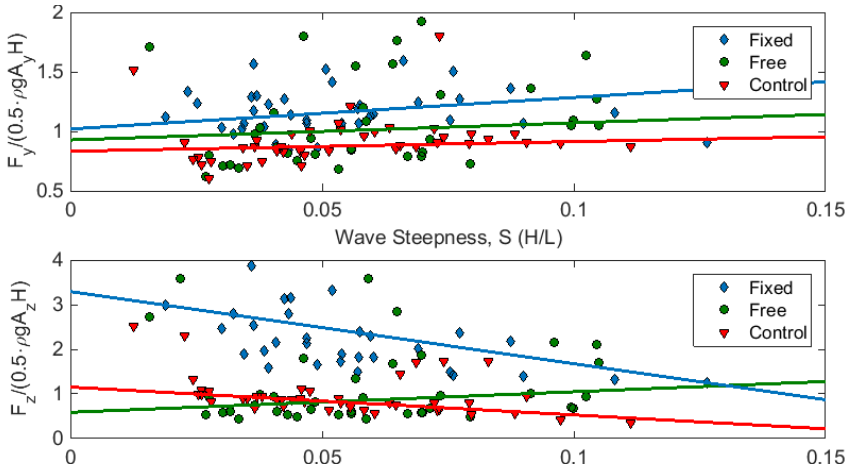

Figure 2.8: Normalized forces on float for the regular wave series.

2.4 Discussion

The regular waves regimes carried out in the experiments was shown in Fig. 2.3. For some of the regular waves with shorter periods this could result in scattering and diffraction of the waves on the device. Using the fundamental Morison's equation in these cases may lead to inaccurate estimate of the load contributions. The effect of diffraction is not examined in this report.
With increasing wave heights the effects of drag increases. Unfortunately the contribution from drag is limited in these experiments. This is due to physical limitations of the basin, wave maker and wave breaking conditions. The wave length would need to exceed 10 m and the height be more than 1 m for the device used.

The effect of the inertia dominated regime is evident in Figs. 2.4b and 2.5b. With increasing Reynold's numbers both the LS and MV methods converges. The estimates are still rough compared to the results from the stream canal (cf. Fig. 2.4b). Due to the inherent scale of drag dominated waves it is unlikely to be a critical factor. With this in mind the found coefficients are considered to be sufficiently accurate.
The scatter with high Reynold's numbers in Fig. 2.4b is curious, it may be partly attributed to uncertainties caused by increasing drag (Dean and Dalrymple (1984)). The spreading of the C_M values in Fig. 2.5b are evidently related to the wave period. This will be examined further in later projects.
The remaining culprits could be the estimation of the particle velocity near the surface of the device, scaling effects or need for additional parameters in the Morison Equation for the low particle velocity regime.

Figs. 2.6 and 2.7 suggests that the control scheme used wont increase the horizontal forces, compared to the fixed and free floating conditions. There is no apparent pattern in the fluctuations that could be anticipated from resonance around the eigenfrequency of the device. The maximum vertical forces are however as great as the case with the float locked in place. By normalizing the results with the Froude-Krylov estimate in Fig. 2.8 and plotting against the wave steepness the only significant outlier is the vertical forces of the fixed float. This is likely explained by the forced submergence of the float leading to increased forces (No changes are made to the wetted surface in the Froude-Krylov forces).

Conclusion

Experiments were carried out in current flume and wave basin. The device used, a 1:40 scale point absorber was subjected to various current velocities and then a wide range of regular waves. From the experiments, the inertia and drag coefficients were estimated using two distinct methods on the float locked in place. The results were compared with result from the canal. Then the float was released from the locked position, and put in two states. First to oscillate freely and then controlled using a PTO. The resulting forces were shown in both vertical and in the wave propagation direction, with respect to wave period and height. Then the results were normalized using Froud-Krylov.

Getting accurate values for both drag and inertia coefficients showed to be difficult in the wave basin. The obtained inertia coefficients generally stays within a reasonable degree of scattering, though particularly in heave the values still vary more than anticipated. The contributions from drag is very small compared to inertia and generally results in poorer estimates. For increasing Reynolds numbers the contribution increases relatively and the results improves noticeably. Near the highest Reynolds values, the drag coefficient in surge that correspond to the value obtained in the stream canal. This should be sufficient to put some confidence in the found values.

Unfortunately, several issues makes it difficult to make any concluding remark on the free and controlled cases. Firstly, the control parameters were never optimized for the wave conditions, and secondly the results found had significant scattering.

Several experiments were dropped due to complications. The small pressure sensors did not produce satisfying results, which were often contradictory and inconsistent. Trying to acquire new and more accurate sensors has been unsuccessful till date. Several sensors has been tested from manufacturers claiming to have appropriate sensors. However, the trade-off between sensitivity and frequency response has been a prevailing issue. Another issue is the thermal response from the sensors during submersion and temporal fluctuations. In the end this was dropped entirely for this small scale device, but was picked up with success at larger scale experiments later. These later experiments also led to the explanation of the vertical inertia-dependency on wave periods.

Bibliography

Brorsen, M. (2007). Non-linear Waves. Technical Report 9, Aalborg University Department of Civil Engineering.

Chakrabarti, S. (1987). *Hydrodynamics of Offshore Structures*. WIT press.

Chaplin, J. R. (1980). Development of stream function wave theory. *Journal of Coastal Engineering*, (2):179–205.

Dean, R. (1965). Stream function representation of nonlinear ocean waves. *J. Geophys. Res.*, 70:4561–4572.

Dean, R. G. and Dalrymple, R. A. (1984). *Water wave mechanics for engineers and scientists*. Prentice-Hall, inc.

Fenton, J. D. (1985). A Fifth-Order Stokes Theory for Steady Waves. *J. Waterway Port Coastal and Ocean Engng*, 111(2):216–234.

Frigaard, P. and Andersen, T. L. (2010). Technical Background Material for the Wave Generation Software AwaSys 5. Technical Report 64, Aalborg University Department of Civil Engineering.

Hansen, R. H. and Kramer, M. M. (2011). Modelling and Control of the Wavestar Prototype. EWTEC European Wave and Tidal Energy Conference.

Kramer, M. M., Marquis, L., and Frigaard, P. (2011). Performance Evaluation of the Wavestar Prototype. EWTEC European Wave and Tidal Energy Conference.

Appendix A

Instrumentation and Data Acquisition in Wave Basin

A.1 The Float and embedded sensors

The components used for the float is shown in Fig. A.1. The pressure sensors used are connected in a junction box inside the float and send through a multi-conductor cable. This solution was chosen to improve the water-sealing of the device. This also meant that the individual cables could be shortened significantly (to ca. 30 cm). This served to reduce the blockage of the air pipe used by the differential pressure sensors. In the past the long cables would twist and constrict airflow through the pipe resulting in slower response. The 13 pressure sensors embedded in the shell are

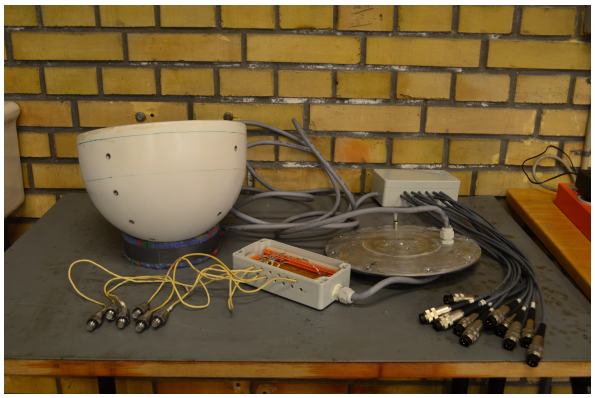

Figure A.1: Disassembled float showing pressure sensors, with the junction box, glass fiber shell and lid.

vented gauges from Kullite. The rated pressure is 1 bar, with a sensitivity of 73 mV/bar. The technical specifications are shown in Fig. A.2. The placement of the pressure sensors are shown on the Fig. A.3. The symmetry lines were chosen to have

redundancy in the measurements.

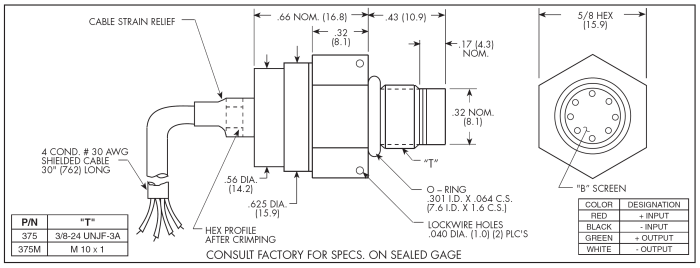

Figure A.2: Pressure sensor specifications. The membrane is 8.1 mm in diameter and ventilated through the attached cable.

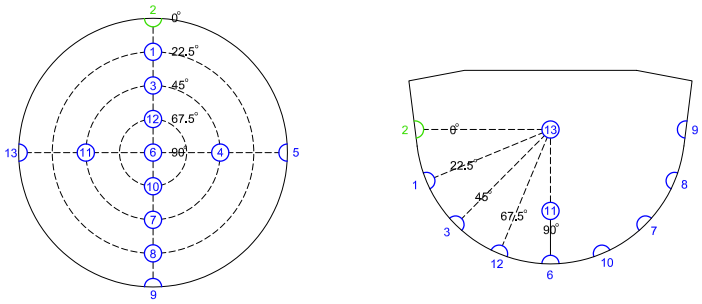

Figure A.3: Pressure sensor placement. Blue and green circles indicates the locations of the sensors. The green marked sensor faces the wave maker.

A.2 Force and Torque transducer

To measure the force and torque on the float a 6-axis sensor is used. This sensor shown in Fig. A.4 is a Delta SI-330-30 from ATI Industrial Automation. The sensor is able to measure forces up to 330 N and torque up to 30 Nm. The accuracy of the sensor is $F_{x,y,z} = 1.5\%$, $M_{x,y} = 1.5\%$ and $M_z = 2.0\%$. A calibration matrix is supplied by the manufacturer. The offset is removed in-situ by applying known loads in all axial directions.

A.3 Simulink and XPC data acquisition

The wave generation software used in the basin is handled using the in-house software AwaSys cf. Frigaard and Andersen (2010).
Data acquisition is handled by a National Instrument Data Acquisition unit (DAQ) which is connected to a dedicated PC running Matlab's Simulink connected to a

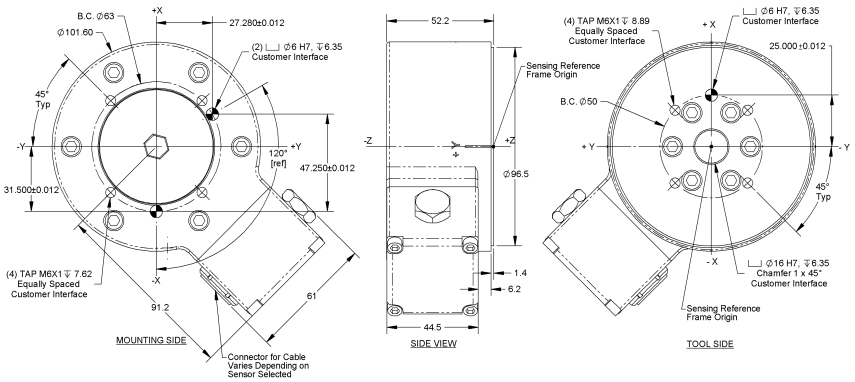

Figure A.4: Six degree of freedom force transducer. Coordinate system and force/moment definition.

remote (target) xPC running a custom operating system. This solution is chosen due to the flexibility and real-time data processing on the xPC. The channel configuration is shown in Table A.1.

Table A.1: DAQ Channel configuration for experiments in wave basin.

Channel	Type	Sym.	Description
00	Force	F_{cyl}	Cylindrical force transducer
01	Force	F_{acc}	Reference force from accelerometer
02	Distance	x_{cyl}	Cylinder position
03	Distance	K	Cylinder arm to pivot
04	Angle	θ_{cyl}	Angular position of cylinder
05	Velocity	$\dot{\theta}_{cyl}$	Angular velocity from angle of rotation
06	Acceleration	$\ddot{\theta}_{cyl}$	Angular acceleration from angular velocity
07	Acceleration	$\ddot{\theta}_{acc}$	Raw angular acc. from accelerometer
08	Acceleration	$\ddot{\theta}_{acc,filt}$	Filtered ang. acc. from accelerometer
09	Power	P	Power produced
10	Trigger		Awasys wave generation trigger
11-26	Elevation	η	Resistive wave gauges
27-39	Pressure	p	Pressure sensors in float shell
40-43	Velocity	u	Acoustic Doppler Velocimeter (ADV)
44-49	Force & moment	FT	6-Axis F/T-transducer

A.4 Surface Elevation and Velocimetry

The placement of the wave gauges and the ADV is shown in Fig. A.5. Wave gauges 8 to 13 and the ADV are placed in line with the float to get the particle velocity and

wave elevation that affects the float. To determine the wave spectrum and separate incident waves from reflected waves from the beach additional wave gauges are placed parallel with the wave propagation direction. To measure the current velocity an

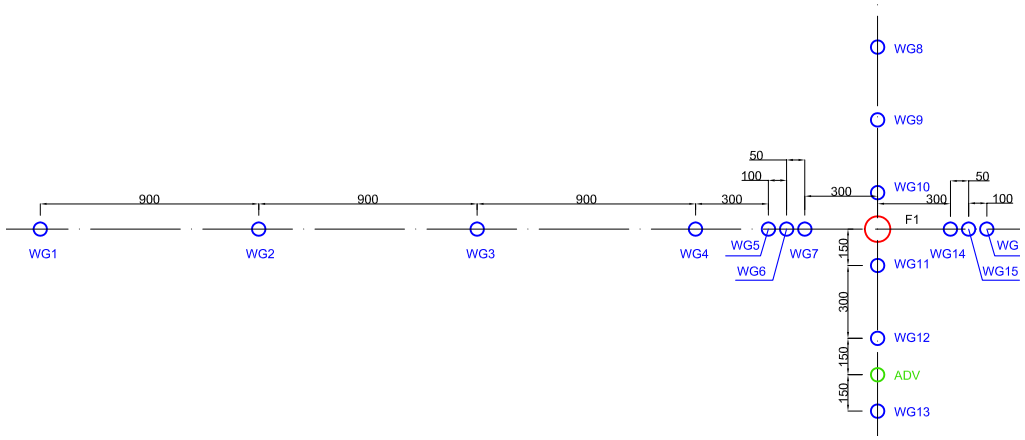

Figure A.5: Layout of wave gauges and floating devices in experiment. The red circle is the float location. The green circle is the ADV used for velocimetry, the blue circles are wave gauges for measurement of wave elevation.

Acoustic Doppler Velocimeter (ADV) from Nortek is used, see Fig. A.6. This device measures particles in the water to determine the velocity and can provide an analogue output to the DAQ. The measuring range used is ±1 m/s with a measurement accuracy of ±0.5%. The ADV is able to measure both the X,Y and two values in the Z direction. To ensure that the ADV does not breach the water surface during the wave troughs the ADV is placed deeper than the largest through. For these experiments this location was determined to be 0.21 m below the mean water level.

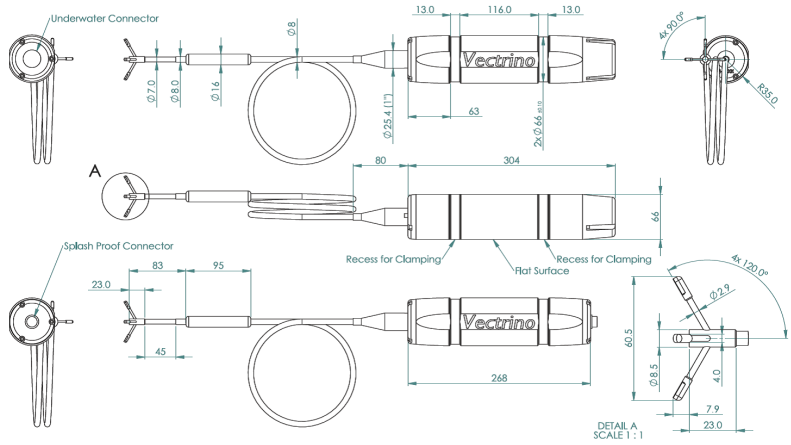

Figure A.6: Dimensions of velocimeter from Nortek.

A.5 The Basin and Wave Series

The wave basin dimensions and location of the float are shown in Fig. A.7. The

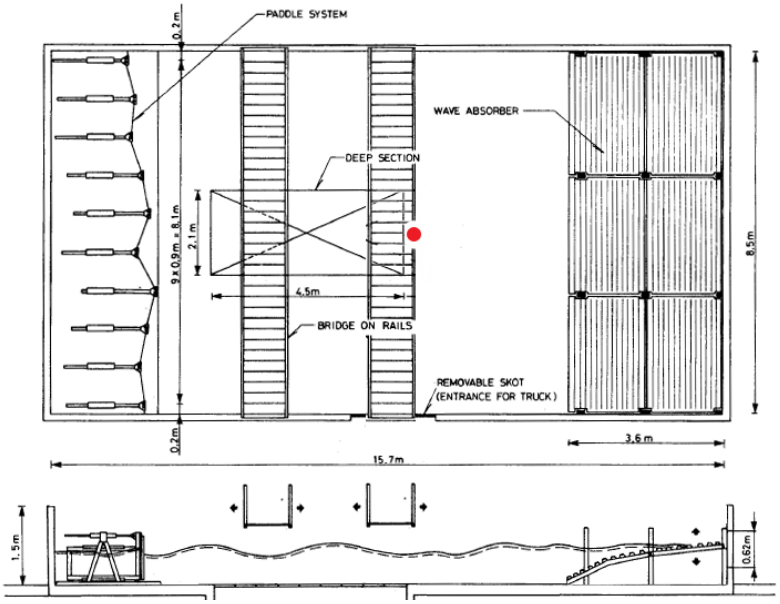

Figure A.7: Sketch of 3D wave basin with floater (red marker) in position.

regular test series which has been used in these tests are given in Table A.2. Each sub-series consist of a single wave period and increasing wave height. The wave makers are set to run each regular wave series for 60 seconds and rest for 45 seconds between each test. This is deemed to be sufficient to calm the basin between each series of regular waves.

Table A.2: Summary of regular waves.

ID	Height, H	Period, T	Length, L	Steepness, S (H/L)
RA01	0.02 m	0.7 s	0.771 m	0.026
RA02	0.04 m	0.7 s	0.785 m	0.051
RA03	0.07 m	0.7 s	0.821 m	0.085
RA04	0.09 m	0.7 s	0.851 m	0.106
RB01	0.03 m	1.0 s	1.552 m	0.019
RB02	0.06 m	1.0 s	1.568 m	0.038
RB03	0.10 m	1.0 s	1.605 m	0.062
RB04	0.14 m	1.0 s	1.654 m	0.085
RB05	0.16 m	1.0 s	1.682 m	0.095
RC01	0.02 m	1.4 s	2.762 m	0.007
RC02	0.07 m	1.4 s	2.777 m	0.025
RC03	0.12 m	1.4 s	2.810 m	0.043
RC04	0.18 m	1.4 s	2.870 m	0.063
RC05	0.22 m	1.4 s	2.920 m	0.075
RC06	0.26 m	1.4 s	2.977 m	0.087
RD01	0.03 m	2.0 s	4.503 m	0.007
RD02	0.10 m	2.0 s	4.539 m	0.022
RD03	0.18 m	2.0 s	4.625 m	0.039
RD04	0.25 m	2.0 s	4.734 m	0.053
RD05	0.31 m	2.0 s	4.845 m	0.064
RE01	0.02 m	0.8 s	1.003 m	0.020
RE02	0.04 m	0.8 s	1.015 m	0.039
RE03	0.05 m	0.8 s	1.023 m	0.049
RE04	0.07 m	0.8 s	1.044 m	0.067
RE05	0.09 m	0.8 s	1.070 m	0.084
RF01	0.02 m	1.2 s	2.153 m	0.009
RF02	0.06 m	1.2 s	2.166 m	0.028
RF03	0.10 m	1.2 s	2.193 m	0.046
RF04	0.14 m	1.2 s	2.232 m	0.063
RF05	0.17 m	1.2 s	2.267 m	0.075
RG01	0.02 m	0.9 s	1.265 m	0.016
RG02	0.04 m	0.9 s	1.274 m	0.031
RG03	0.06 m	0.9 s	1.288 m	0.047
RG04	0.08 m	0.9 s	1.308 m	0.061
RG05	0.10 m	0.9 s	1.332 m	0.075
RH01	0.02 m	1.1 s	1.848 m	0.011
RH02	0.05 m	1.1 s	1.858 m	0.027
RH03	0.07 m	1.1 s	1.870 m	0.037
RH04	0.11 m	1.1 s	1.904 m	0.058
RH05	0.14 m	1.1 s	1.938 m	0.072
RI01	0.02 m	1.3 s	2.458 m	0.008
RI02	0.05 m	1.3 s	2.466 m	0.020
RI03	0.09 m	1.3 s	2.487 m	0.036
RI04	0.13 m	1.3 s	2.520 m	0.052
RI05	0.17 m	1.3 s	2.562 m	0.066
RJ01	0.02 m	1.5 s	3.061 m	0.007